OPEN

Deficiency of Parkinson's disease-related gene *Fbxo7* is associated with impaired mitochondrial metabolism by PARP activation

Marta Delgado-Camprubi[1,2], Noemi Esteras[1,2], Marc PM Soutar[1], Helene Plun-Favreau*[1,3] and Andrey Y Abramov*[1,3]

The Parkinson's disease (PD)-related protein F-box only protein 7 (Fbxo7) is the substrate-recognition component of the Skp1-Cullin-F-box protein E3 ubiquitin ligase complex. We have recently shown that PD-associated mutations in *Fbxo7* disrupt mitochondrial autophagy (mitophagy), suggesting a role for Fbxo7 in modulating mitochondrial homeostasis. Here we report that Fbxo7 deficiency is associated with reduced cellular NAD$^+$ levels, which results in increased mitochondrial NADH redox index and impaired activity of complex I in the electron transport chain. Under these conditions of compromised respiration, mitochondrial membrane potential and ATP contents are reduced, and cytosolic reactive oxygen species (ROS) production is increased. ROS activates poly (ADP-ribose) polymerase (PARP) activity in Fbxo7-deficient cells. PARP inhibitor restores cellular NAD$^+$ content and redox index and ATP pool, suggesting that PARP overactivation is cause of decreased complex I-driven respiration. These findings bring new insight into the mechanism of Fbxo7 deficiency, emphasising the importance of mitochondrial dysfunction in PD.
Cell Death and Differentiation (2017) **24,** 120–131; doi:10.1038/cdd.2016.104; published online 30 September 2016

Mitochondrial susceptibility to age-related oxidative stress makes mitochondrial impairment a common feature of neurodegeneration.[1] Parkinson's disease (PD) is the most common neurodegenerative movement disorder affecting 1% of the world population above the age of 60.[2] Evidence of mitochondrial dysfunction in PD derives from mitochondrial toxin-induced models of the disease,[3,4] and from the observation of mitochondrial abnormalities in post-mortem tissue from patients with idiopathic PD.[5–7] Mutations in disease-related genes encoding for proteins with a mitochondrial function have also been identified, further supporting the conclusion that mitochondrial impairment is a hallmark of PD.[8–11]

Mutations in the F-box only protein 7 gene (*Fbxo7; PARK15*) cause autosomal recessive juvenile atypical Parkinsonism with pyramidal syndrome.[12] Fbxo7 belongs to a sub-class of F-box proteins (FBPs) that function as adaptors for the Skp1-Cullin-F-box (SCF) class of ubiquitin E3 ligases. SCF complexes are involved in the phosphorylation-dependent ubiquitination of proteins targeted for proteasomal degradation.[13] FBPs determine the specificity of the substrate to be ubiquitinated by bringing the substrate into proximity with the SCF complex.[14] In addition to SCF-dependent activities, several FBPs participate in cellular functions, including cell cycle regulation and mitochondrial dynamics.[15] We have recently shown that, together with the PD-associated proteins, PTEN-induced putative kinase 1 (*PARK6*) and Parkin (*PARK2*), Fbxo7 regulates the selective autophagic clearance of depolarised mitochondria (mitophagy). Although predominantly detected at the mitochondria upon depolarisation, a small proportion of Fbxo7 is present in non-depolarised mitochondria, suggesting a potential role for Fbxo7 in regulating basal mitochondrial homeostasis.[16]

Poly (ADP-ribose) (PAR) polymerase (PARP) enzymes activate DNA repair in response to oxidative damage by mediating the attachment of PAR polymers on itself and other proteins. The PARP family includes 18 members, among which PARP-1 (hereafter referred as PARP) is responsible for the 80% of the NAD$^+$-dependent synthesis of PAR polymers.[17] PARP prolonged activation can, however, cause a reduction of cellular NAD$^+$, which in turn can lead to ATP reduction and bioenergetic collapse.[18] PARP-activated NAD$^+$ depletion has been associated before with the pathogenesis of neurodegenerative disorders, in particular with Alzheimer's disease[19–21] and glutamate excitotoxicity.[22,23]

In this study, we sought to investigate the mitochondrial pathophysiology associated with Fbxo7 deficiency in *Fbxo7* knockdown (KD) human dopaminergic neuroblastoma SH-SY5Y cells and in patient fibroblasts harbouring the homozygous R378G pathogenic mutation in *Fbxo7*. We report that Fbxo7 deficiency is associated with cellular NAD$^+$ depletion, limiting NADH substrate for complex I in the mitochondrial

[1]Department of Molecular Neuroscience, UCL Institute of Neurology, Queen Square, London, UK
*Corresponding author: AY Abramov or H Plun-Favreau, Department of Molecular Neuroscience, UCL Institute of Neurology, Queen Square, London WC1N 3BG, UK. Tel: +44 2078 3736 11; Fax: +44 2072 785 616; E-mail: a.abramov@ucl.ac.uk or h.plun-favreau@ucl.ac.uk
[2]Joint first authors.
[3]These authors contributed equally to this work.

electron transport chain (ETC). Fbxo7 deficiency results in impaired complex I-linked respiration, limited maximal oxygen rate capacity and mitochondrial depolarisation. We found that Fbxo7 deficiency leads to the activation of PARP. We show that PARP pharmacologic inhibition increases cellular NAD^+ levels, and restores NADH redox index and complex I NADH dehydrogenase activity that results in recovery of the ATP pool in *Fbxo7*-deficient cells. Our findings suggest that PARP overactivation may cause mitochondrial dysfunction in Fbxo7-deficient cells.

Results

Mitochondrial membrane potential and ATP levels are reduced in Fbxo7-deficient cells.

Mitochondrial membrane potential ($\Delta\Psi m$) can be measured using tetramethylrhodamine methyl ester (TMRM) to estimate mitochondrial function and cell health.[24] Whenever possible, all experiments were performed in two different cell models of Fbxo7 deficiency (patient's fibroblasts and KD SH-SY5Ys), in order to exclude any artefact due to a particular cell genetic background. To study Fbxo7's role in mitochondrial maintenance, $\Delta\Psi m$ was measured in a stable *Fbxo7* KD SH-SY5Y cell line and in a fibroblast line derived from a PD patient with the *Fbxo7* R378G mutation (Figure 1ai–ii). In both models, Fbxo7 deficiency was associated with a significant reduction in the TMRM fluorescence as compared with controls (Figure 1bi; $15.6 \pm 3.6\%$ reduction, $n = 4$, $P < 0.05$; Figure 1bii; $37.6 \pm 5.4\%$ decrease compared to control 1, $n = 4$, $P < 0.05$; $48.9 \pm 22.5\%$ decrease compared with control 2, $n = 4$; $P < 0.05$). The level of Fbxo7 KD was estimated at 90% by western blot (WB; Supplementary Figure S1Ai).

When the proton pumps of the ETC are not sufficient to maintain $\Delta\Psi m$, the ATP synthase can work in reverse mode to sustain the proton gradient by ATP hydrolysis.[25,26] To investigate the mechanism of $\Delta\Psi m$ maintenance in Fbxo7 deficiency, cells were treated with different mitochondrial toxins. Treating control and Fbxo7-deficient cells with 2 μg/ml of oligomycin, an inhibitor of the F_1F_0-ATP synthase, caused no depolarisation, indicating that the ATP synthase is not working in reverse mode. Subsequent addition of complex I inhibitor, rotenone (5 μM), resulted in a profound depolarisation, followed by a complete depolarisation after addition of the mitochondrial uncoupler carbonylcyanide-*p*-trifluoromethoxyphenylhydrazone (FCCP; 1 μM). These data indicate that in Fbxo7-deficient cells, $\Delta\Psi m$ is maintained by the ETC activity as opposed to ATP hydrolysis (Supplementary Figure S1B).

Reduction in $\Delta\Psi m$ may suggest a disruption of the ATP content, which was reduced in *Fbxo7* KD SH-SY5Y cells when compared with scrambled (scr) cells (Figure 1ci; $14 \pm 4.5\%$ reduction; $n = 3$; $P < 0.05$). ATP levels were significantly decreased in fibroblasts carrying the *Fbxo7* mutation as compared with control fibroblasts (Figure 1cii; $21 \pm 6.8\%$ reduction compared with control 1, $n = 5$, $P < 0.05$; $47.1 \pm 6.8\%$ reduction compared with control 2, $n = 3$, $P < 0.05$), indicating that Fbxo7 deficiency is associated with decreased cellular ATP levels.

Oxygen consumption is disrupted in *Fbxo7* KD SH-SY5Ys.

A reduction in $\Delta\Psi m$ and cellular ATP in Fbxo7-deficient cells suggests a potential respiratory defect. To investigate the cell respiratory activity, the rate of oxygen consumption was measured using a Clark oxygen electrode in a clonal population of cells stably expressing scr or Fbxo7 shRNA. Rates of basal oxygen consumption were similar in scr and in *Fbxo7* KD cells (Figure 2a; 2.4 ± 0.4 ng $O/min/10^6$ scr cells; 2.6 ± 0.2 ng $O/min/10^6$ KD cells, $n = 12$). Addition of oligomycin (2 μg/ml) inhibited oxygen consumption in both cell types to a similar extent (Figure 2a; 0.6 ± 0.1 ng $O/min/10^6$ scr cells; 0.8 ± 0.1 ng $O/min/10^6$ KD cells, $n = 11$), indicating that neither inhibition of respiration nor uncoupling under basal conditions occurs in Fbxo7-deficient cells. Subsequent treatment with FCCP (1 μM) induced an increase in oxygen consumption in scr and in *Fbxo7* KD SH-SY5Ys, but only to a much lesser extent in the later (Figure 2a; 14.4 ± 2.2 ng $O/min/10^6$ scr cells; 6.1 ± 1.2 ng $O/min/10^6$ KD cells; $n = 7$, $P < 0.01$), indicating that Fbxo7 deficiency is associated with reduced maximal rates of oxygen consumption.

To further investigate the ETC activity and its coupling to oxidative phosphorylation, oxygen consumption was examined in detergent-permeabilised SH-SY5Ys (40 μM digitonin). Cell permeabilisation allows the study of the individual contribution of specific respiratory complexes to respiration in the presence of their substrates.[24] To measure the rate of oxygen consumption in state III (V3; ADP-stimulated respiratory state) and state IV (V4), 50 nmol ADP was added following the addition of complex I substrates (5 mM glutamate and 5 mM malate) or complex II substrates (5 mM succinate in the presence of 5 μM rotenone). V4 is the respiratory rate reached after state III when added ADP is consumed and the rate of oxygen consumption returns close to pre-ADP values. The respiratory control ratio (RCR) is calculated as the ratio V3/V4, and is an indication of the degree of coupling between respiration and oxidative phosphorylation. The RCR showed no significant difference between both cell populations, confirming that loss of Fbxo7 is not associated with mitochondrial uncoupling (Figure 2b; 1.9 ± 0.03 V3/V4 in scr cells; 1.9 ± 0.2 V3/V4 in KD cells after addition of glutamate, $n = 3$; 1.5 ± 0.1 V3/V4 in scr cells; 1.7 ± 0.1 V3/V4 in KD cells after addition of succinate, $n = 3$). Rates of respiration in V3 and V4 were also similar in the presence of succinate in control and KD cells (Figures 2c and d; V3: 122 ± 23.4 ng $O/min/10^6$ scr cells; 149.6 ± 34.4 ng $O/min/10^6$ KD cells; V4: 85.5 ± 10.9 ng $O/min/10^6$ scr cells; 101.1 ± 16.9 ng $O/min/10^6$ KD cells; $n = 3$). However, V3 and V4 respiration rates were significantly reduced in the presence of glutamate or malate in *Fbxo7* KD cells when compared with control cells (Figures 2c and d; V3: 237.6 ± 21.8 ng $O/min/10^6$ scr cells; 136.6 ± 14.2 ng $O/min/10^6$ KD cells, $n = 4$, $P < 0.01$; V4: 127.9 ± 11.5 ng $O/min/10^6$ scr cells; 67.4 ± 9.1 ng $O/min/10^6$ KD cells; $n = 4$, $P < 0.01$), indicating that, though coupled, Fbxo7-deficient cells have reduced complex I-driven respiration.

Fbxo7 deficiency is associated with lower NADH dehydrogenase activity and increased cytosolic ROS production.

Possible reasons for complex I respiratory impairment include a reduction in protein expression or a
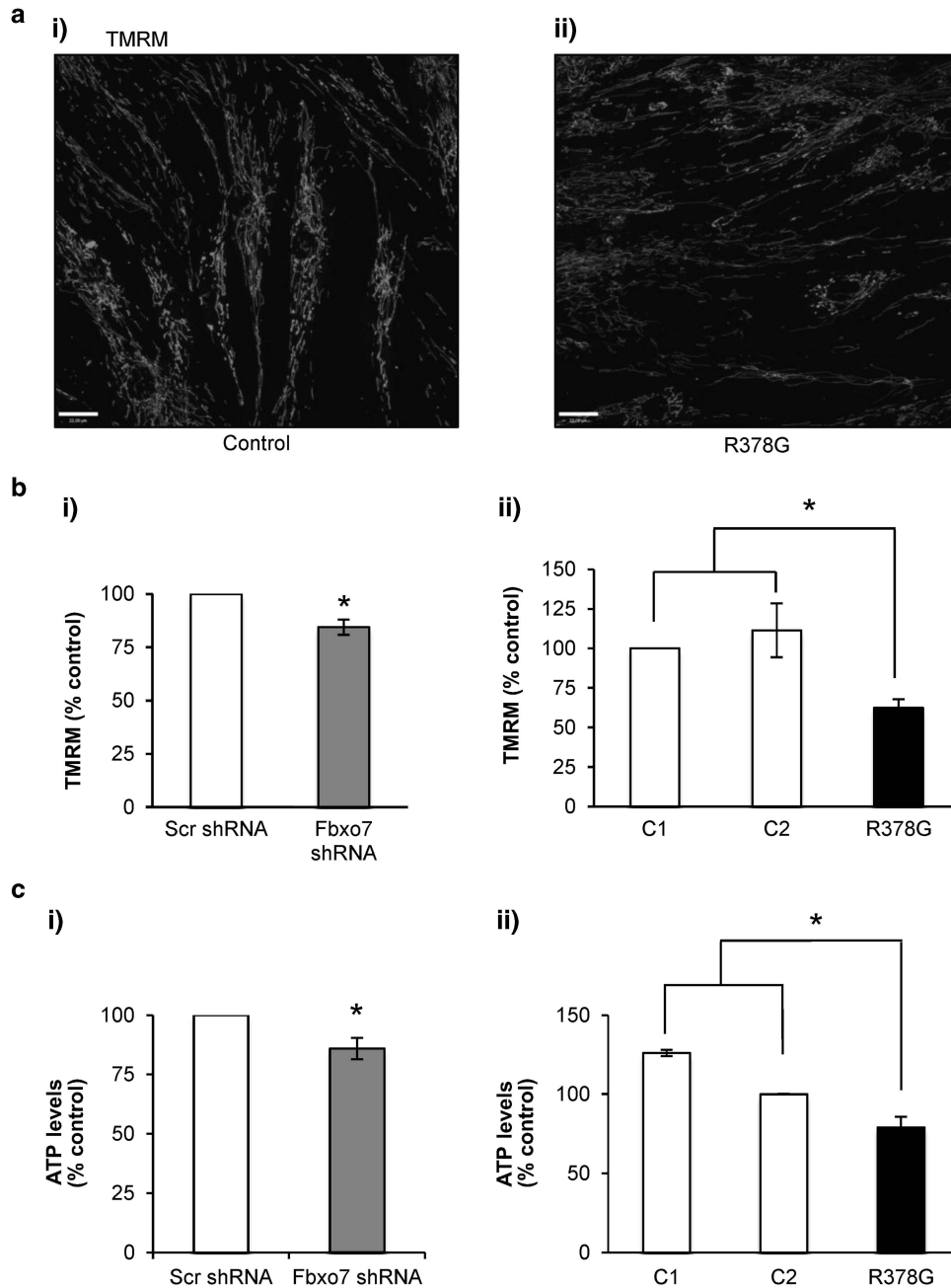
Figure 1 Mitochondrial membrane potential and cellular ATP levels are reduced in Fbxo7-deficient cells. (**a**) ΔΨm was assessed using TMRM (25:nM) in (**a**i) control and (**a**ii) patient fibroblasts, carrying a homozygous *Fbxo7* R378G mutation and SH-SY5Y cells stably expressing either scr or Fbxo7 shRNA (data not shown). (**b**) Histograms represent average TMRM intensity in SH-SY5Y cells (**b**i) and patients fibroblasts (**b**ii) normalised to control cells, respectively. Data are represented as mean ± S.E.M. from four independent experiments. In all cases, * indicates $P < 0.05$ compared with control values. The specificity of Fbxo7 antibody and KD were confirmed by WB (Supplementary Figure S1A). (**c**) Total ATP levels were determined using a luciferase assay kit (Vialight plus assay kit (Lonza, Verviers, Belgium)) based on the bioluminescent measurement of ATP and samples were referred to an ATP standard curve. Histograms represent average ATP levels per protein concentration, normalised to control cells in SH-SY5Y cells stably expressing either (**c**i) scr or Fbxo7 shRNA, and (**c**ii) control and patient fibroblasts with *Fbxo7* R378G mutation. Data are represented as mean ± S.E.M. from three (SH-SY5Ys) and five (fibroblasts) independent experiments; *$P < 0.05$

decrease in its enzymatic activity. To investigate complex I protein levels in Fbxo7-deficient cells, cell lysates from *Fbxo7* KD SH-SY5Ys and from PD patient fibroblasts were assessed by WB using a cocktail of antibodies directed against subunits of complexes I–V of the ETC. No difference in the protein expression of these complexes subunits was detected between Fbxo7-deficient cells and controls (Figure 3a), indicating that impaired respiration associated with Fbxo7 deficiency is not related to reduced expression of the ETC proteins. The decrease in complex I-driven respiration observed in whole and permeabilised Fbxo7-deficient cells might, however, arise from a reduction in complex I activity.
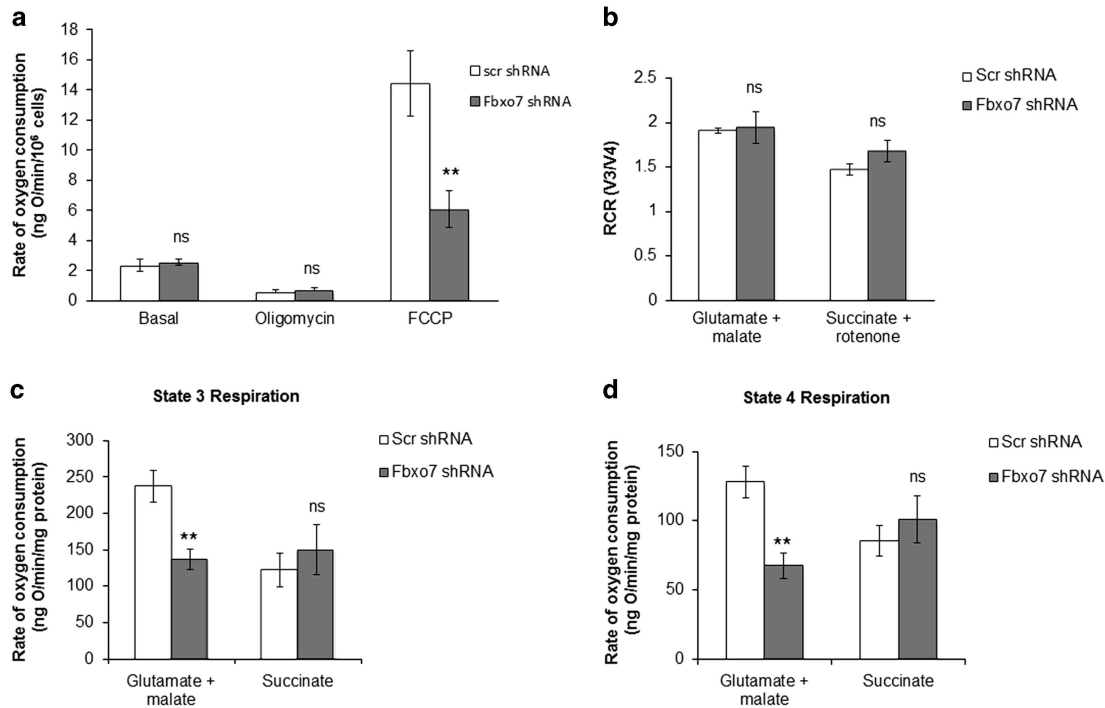
Figure 2 Oxygen consumption is disrupted in *Fbxo7* KD SH-SY5Y cells. (**a**) Rate of oxygen consumption was measured using a Clark oxygen electrode in SH-SY5Y cells, expressing either scr or Fbxo7 shRNA under basal conditions and following addition of oligomycin (2 μg/ml) and FCCP (1 μM). Cells were permeabilised with digitonin (40 μM) before measuring oxygen consumption in state III (ADP stimulated) (**c**) and state IV (no ADP present) (**d**) in the presence of substrates for complex I (glutamate and malate, 5 mM) or complex II (succinate 5 mM in the presence of rotenone 5 μM). (**b**) RCR (the ratio of state III to state IV) was calculated for control and *Fbxo7* KD SH-SY5Y cells. Data are represented as mean ± S.E.M. from at least three independent experiments; ** indicates $P < 0.01$, NS, not significant compared with control values

Complex I NADH dehydrogenase activity was measured kinetically over 30 min and the rate was determined as changes in optical density over time. A significant decrease in complex I activity was observed in *Fbxo7* KD cells when compared with control cells (Figure 3bi; 22.6 ± 5.4% decrease; $n = 5$; $P < 0.01$). The linear rate of absorbance increase in patient fibroblasts was also reduced compared to control cells (Figure 3bii; 50.9 ± 2.5% decrease compared with control 1, $n = 3$, $P < 0.01$; 56.7 ± 2.5% decrease compared to control 2, $n = 3$; $P < 0.01$). These data indicate that Fbxo7 deficiency is associated with altered NADH dehydrogenase activity of isolated complex I.

Studies in various models have shown that complex I respiratory impairment is associated with increased reactive oxygen species (ROS) production.[27–29] To investigate whether ROS levels are increased in Fbxo7 deficient cells, cytosolic ROS production was measured in live cells using the fluorescent indicator dihydroethidium (DHE; Figure 3c). Basal level of cytosolic ROS production was significantly higher in *Fbxo7* KD SH-SY5Ys and in patient fibroblasts as compared with controls (Figure 3di; 1.01 ± 0.4 increase in KD cells; $n = 8$; $P < 0.05$; Figure 3dii; 0.57 ± 0.3 increase in mutant fibroblasts compared to control 1; $n = 7$; $P < 0.05$).

Mitochondrial NADH and FAD redox states are altered, and cellular NAD$^+$ content is reduced in Fbxo7-deficient cells. To further investigate the cause of reduced complex I activity in Fbxo7-deficient cells, we examined whether this may arise from a limited NADH supply to complex I in these cells.

NADH is the electron donor for complex I, and as such, NADH levels correlate inversely with respiratory chain activity, although FADH reflects complex II activity (measured as FAD autofluorescence). In order to measure redox indexes, we added FCCP (1 μM) to maximise respiration and thus minimise the NADH pool (and maximise FAD), then added NaCN (1 mM) to block mitochondrial respiration and therefore maximise the NADH pool (and minimise FAD). The initial NADH or FAD autofluorescence (or redox state) is then calculated as a percentage of this range (Figure 4a–c). In addition, the total mitochondrial pool of NADH or FAD (maximum autofluorescence minus minimum) may be taken as an indication of the substrate availability for complexes I and II, respectively.[30,31]

NADH redox index was higher in *Fbxo7* KD SH-SY5Ys and in patient fibroblasts as compared with controls (Supplementary Figure S2A; 72.9 ± 3.2% in SH-SY5Y *Fbxo7* KD cells; 53.6 ± 1.9% in scr cells, $n = 14$; $P < 0.001$; Supplementary Figure S2Aii; 50.6 ± 4.5% in patient fibroblasts; 31.7 ± 2.7% in control 1; 32.7 ± 3% in control 2, $n = 14$; $P < 0.01$), indicating that the NADH redox index is closer to the maximally reduced state in Fbxo7-deficient cells. These results are consistent with a possible decreased complex I respiration rate. The FAD^{++} redox index was also increased in *Fbxo7* KD SH-SY5Ys as compared with scr cells (Figures 4c and d; 72.9 ± 7.8% in Fbxo7 KD cells; 31.6 ± 2.5% in scr cells, $n = 4$; $P < 0.01$), indicating an increase in complex II activity, possibly to counteract complex I deficiency. It was not possible to measure FAD^{++} autofluorescence in fibroblasts due to their low levels of FAD^{++} autofluorescence.
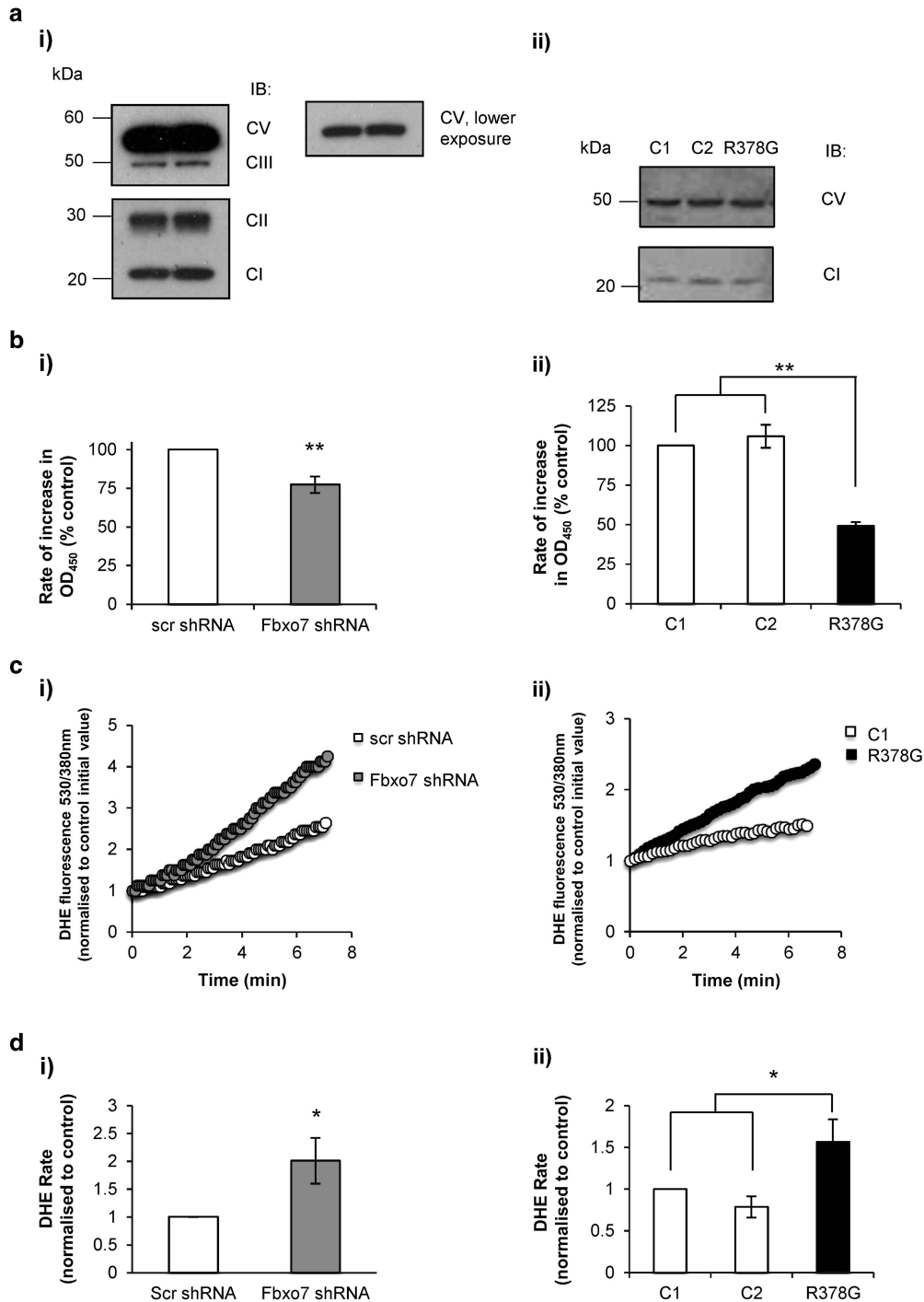
Figure 3 Fbxo7 deficiency is associated with lower NADH dehydrogenase activity and increased cytosolic ROS production. (**a**) Lysates from SH-SY5Y cells expressing either scr or Fbxo7 shRNA (**ai**) and control and patient fibroblasts with *Fbxo7* R378G mutation (**aii**) were assessed by WB using a cocktail of antibodies against complex I subunit NDUFB8, complex II subunit 30 kDa, complex III core protein 2, complex IV subunit I and complex V α subunit. Complex IV is not detected in cell lysates heated at 100 °C. Abbreviations: CI, complex I; CII, complex II; CIII, complex III; CV, complex V. The experiment was performed three times in independent days. (**b**) Histograms represent average complex I NADH dehydrogenase activity, as measured by rate of increase in absorbance OD_{450}, normalised to control cells from five independent experiments in (**bi**) SH-SY5Y cells and three in (**bii**) fibroblasts. Data are represented as mean $\pm$ S.E.M.; $^{**}P > 0.01$. (**c**) The rate of cytosolic ROS production was assessed by measuring the rate of increase in fluorescence at 530 nm/380 nm in SH-SY5Y cells expressing either (**ci**) scr or Fbxo7 shRNA and (**cii**) control and patient fibroblasts with *Fbxo7* R378G mutation loaded with DHE (80 μM). (**d**) Histograms represent the mean rate of increase in DHE fluorescence in (**di**) SH-SY5Y cells and (**dii**) fibroblasts, expressed as a percentage of control, $\pm$ S.E.M. from at least seven independent experiments; $^*P < 0.05$

The NADH mitochondrial pool was significantly lower in *Fbxo7* KD cells when compared with scr cells (Figure 4di; $38.9 \pm 13\%$ decrease; $n = 4$; $P < 0.01$), and in patient fibro-blasts when compared with control fibroblasts (Figure 4dii; $15.6 \pm 2.9\%$ decrease; $n = 12$; $P < 0.05$), indicating a decrease in NADH oxidation. FAD^{++} mitochondrial pool was increased in
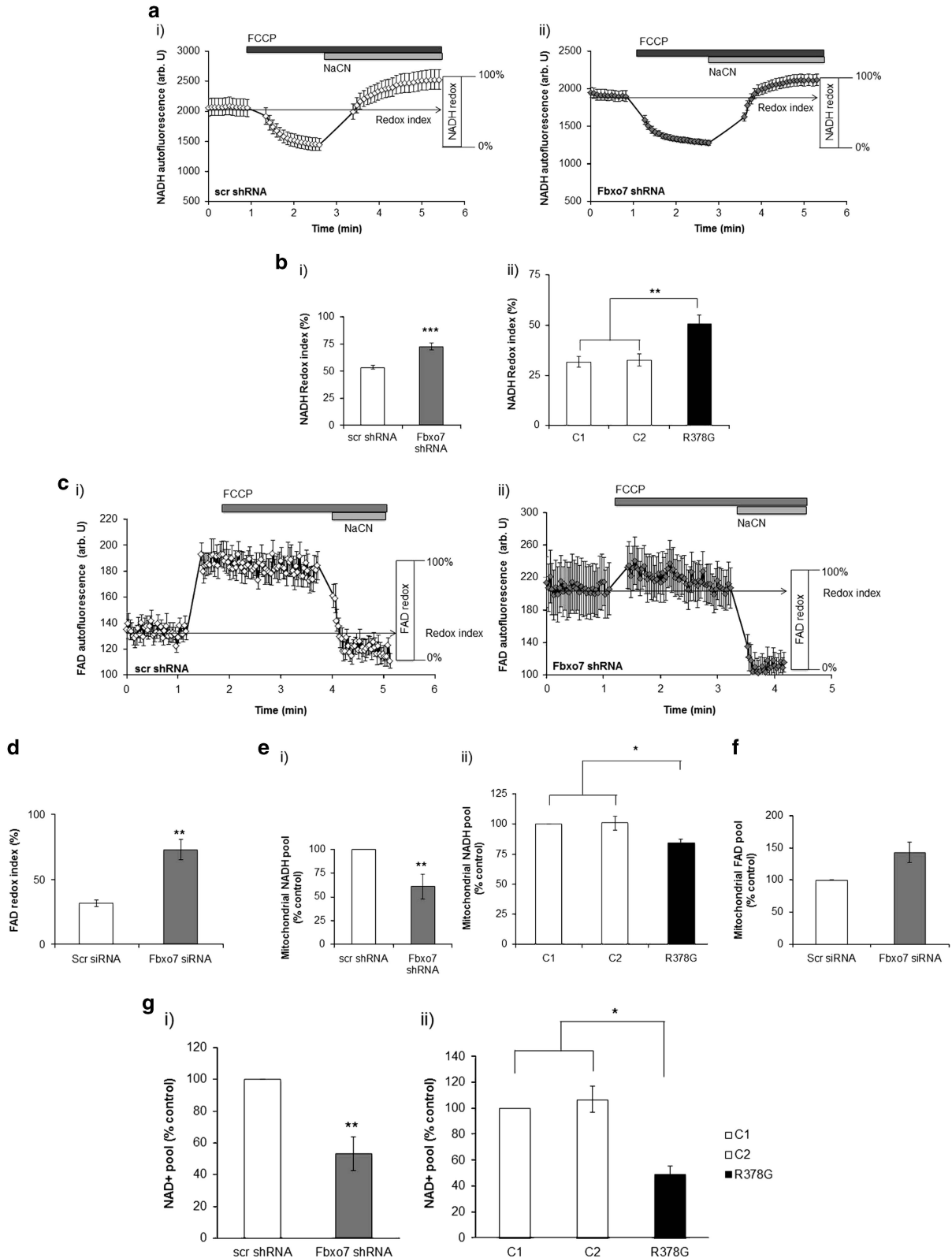

Figure 4 For caption please refer page 126

Fbxo7 KD cells (Figure 4f; 43 ± 15.7% increase; *n* = 3), indicating an increase in FADH$_2$ oxidation. This increase could result from increased complex II activity to compensate for complex I impairment. The reduction in NADH mitochondrial pool may result from impairment upstream of the ETC. One possibility is that the cellular NAD$^+$ pool available to generate NADH in the tricarboxylic acid cycle may be decreased.

A colorimetric cell-based assay kit (Cayman Chemical, Ann Arbor, MI, USA) was used to determine cellular NAD$^+$ levels in Fbxo7-deficient cells. In both *Fbxo7* KD SH-SY5Ys and in patient fibroblasts, NAD$^+$ levels were decreased when compared with controls (Figure 4gi; 46.9 ± 10.8% decrease in *Fbxo7* KD SH-SY5Ys compared with scr cells; *n* = 7; *P* < 0.001; Figure 4gii; 50.7 ± 6.2% decrease in patient fibroblasts compared with control 1 and 57.5 ± 6.2% decrease compared with control 2; *n* = 8; *P* < 0.01), suggesting that decreased cellular NAD$^+$ pool may be the reason for decreased complex I-driven respiration in these cells.

DPQ PARP inhibitor increases cellular NAD$^+$ pool and restores NADH redox index in Fbxo7-deficient cells.

NAD$^+$-consuming proteins include PARPs, whose function has been described to play a role in energy metabolism, cell survival and aging.[19,32] Although PARP activity is important for cell survival, sustained activation can compromise NAD$^+$ bioavailability and deplete intracellular levels, eventually leading to metabolic collapse and cell death.[33–36] Accordingly, PARP inhibitors such as 3,4-dihydro-5-[4-(1-piperidinyl) butoxyl]-1(2H)-isoquinolinone (DPQ), have been described to have a protective function in inflammatory and ischaemia-related disorders.[37–39]

To investigate whether the observed increase in NADH redox index and reduction in NAD$^+$ content in Fbxo7-deficient cells was a result of PARP upregulation, SH-SY5Ys and fibroblasts were treated for 24 h with DPQ (10 μM), before the measurement of the cellular NAD$^+$ pool and NADH redox index. DPQ treatment resulted in a significant increase in cellular NAD$^+$ content in SH-SY5Ys (Figure 5ai; 121 ± 35.1% increase in treated *Fbxo7* KD cells compared with non-treated KD cells; *n* = 4; *P* < 0.01), and in patient fibroblasts (Figure 5aii; 43.2 ± 9.5% increase in treated patient fibroblasts compared with non-treated patient fibroblasts, *n* = 6; *P* < 0.01). DPQ treatment also resulted in a significant decrease in NADH redox index in *Fbxo7* KD SH-SY5Ys and a decrease in patient fibroblasts to similar levels found in non-treated control cells (Figure 5bi; 24.2 ± 2.7% decrease in DPQ-treated KD cells compared with non-treated KD cells, *n* = 9; *P* < 0.01. Figure 5bii; 9.8 ± 3.7% decrease in DPQ-treated patient

cells compared with non-treated patient fibroblasts; *n* = 12). Treatment with DPQ resulted in a significant increase of mitochondrial NADH pool in *Fbxo7* KD cells and in patient fibroblasts (Figure 5ci; 82 ± 13.1% increase in DPQ-treated *Fbxo7* KD cells compared with KD non-treated cells, *n* = 4, *P* < 0.01. Figure 5cii; 15.7 ± 5.7% increase in DPQ-treated patient fibroblasts compared with non-treated patient fibroblasts, *n* = 12, *P* < 0.05). These data show that PARP inhibition restores cellular NAD$^+$ pool and NADH redox index in Fbxo7-deficient cells, suggesting that PARP upregulation is the likely cause of complex I-reduced respiration in these cells.

In order to confirm these results, we measured the protein levels of PARP in control and *Fbxo7* KD cells by WB. We found no difference in protein level between Fbxo7-deficient and control cells (Figure 5di–ii). PARP activity in *Fbxo7* KD cells was significantly higher than in control cells (113.17 ± 0.87% of control; *n* = 4; *P* < 0.05; Figure 5ei). Similar effect was also observed in the mutant fibroblasts (125.40 ± 3.79%, *n* = 4; compared to control 1, 104.67 ± 4.46, *P* < 0.05; and control 2, 95.33 ± 4.46, *P* < 0.01; Figure 5eii). Importantly, inhibitor DPQ (10 μM) blocked this overactivation in Fbxo7-deficient cells (Figure 5ei–ii).

DPQ restores complex I activity in Fbxo7-deficient cells.

To investigate whether PARP upregulation is the cause for decreased complex I activity in Fbxo7 deficiency, SH-SY5Ys and fibroblasts were treated for 24 h with DPQ (10 μM) before measuring complex I NADH dehydrogenase activity. Complex I activity after DPQ pre-treatment was increased in *Fbxo7* KD cells to similar levels of scr non-treated cells (Figure 6ai; 5.1 ± 7% difference compared to scr non-treated cells, *n* = 3). Complex I activity in patient fibroblasts was also significantly increased after DPQ treatment (Figure 6aii; 48 ± 5.5% increase compared with non-treated patient cells; *n* = 3; *P* < 0.01). These data indicate that reduced complex I-driven respiration in Fbxo7-deficient cells is caused by PARP upregulation and that inhibition of PARP activity restores complex I NADH dehydrogenase activity.

Inhibition of PARP restores ATP pool in Fbxo7-deficient cells.

We next investigated the effect of Fbxo7 deficiency and role of the PARP on cellular ATP levels. Mag-Fura is a fluorescent chelator of divalent cations, with a high affinity for magnesium and a much lower affinity for calcium. Consider this it can be used both to investigate ATP levels in individual cells, as ATP binds magnesium and therefore ATP levels are inversely proportional to free magnesium, and to investigate cytotoxicity in response to ATP depletion, as under these conditions the cell is no longer able to maintain its ionic

---

Figure 4 Loss of Fbxo7 function affects mitochondrial NADH and FAD^{++} redox states, and reduces cellular NAD$^+$ content in Fbxo7 KD SH-SY5Y cells. (**a**) The mean of NADH representative traces is shown for SH-SY5Y cells expressing either scr (*n* > 15 cells; **ai**) or Fbxo7 shRNA (*n* > 15 cells; **aii**) following addition of FCCP (1 μM) and NaCN (1 mM). (**b**) Redox index was calculated as a % of the min and max of autofluorescence in SH-SY5Y cells and fibroblasts. (**c**) FAD^{++} representative mean traces (*n* > 20 cells) are shown for SH-SY5Y cells either expressing scr or Fbxo7 shRNA following addition of FCCP (1 μM) and NaCN (1 mM). (**d**) FAD redox index was calculated as a % of the min and max of autofluorescence in scr and *Fbxo7* KD SH-SY5Y cells. (**e**) Mitochondrial NADH pool was calculated and normalised to control SH-SY5 cells and control fibroblasts. (**f**) Mitochondrial FAD^{++} pool was calculated and normalised to control cells. Transient *Fbxo7* KD was confirmed by WB (S2B). Data are represented as mean ± S.E.M. from at least three independent experiments; *P* < 0.05; **P* < 0.01; ***P* < 0.005; NS, not significant. (**g**) Total NAD$^+$ levels were determined measuring the increase in absorbance at 450 nm based on the formation of formazan coupled to the reduction of NAD$^+$ and samples were referred to a NAD$^+$ standard curve. Histograms represent average cellular NAD$^+$ content ± S.E.M per protein concentration normalised to control cells in SH-SY5Y cells stably expressing either (**gi**) scr or Fbxo7 shRNA and (**gii**) control, and patient fibroblasts with *Fbxo7* R378G mutation; **P* < 0.01; *P* < 0.05; *n* > 7 independent experiments. i - representing data for SH-SY5Y cells, ii - data for patients fibroblasts
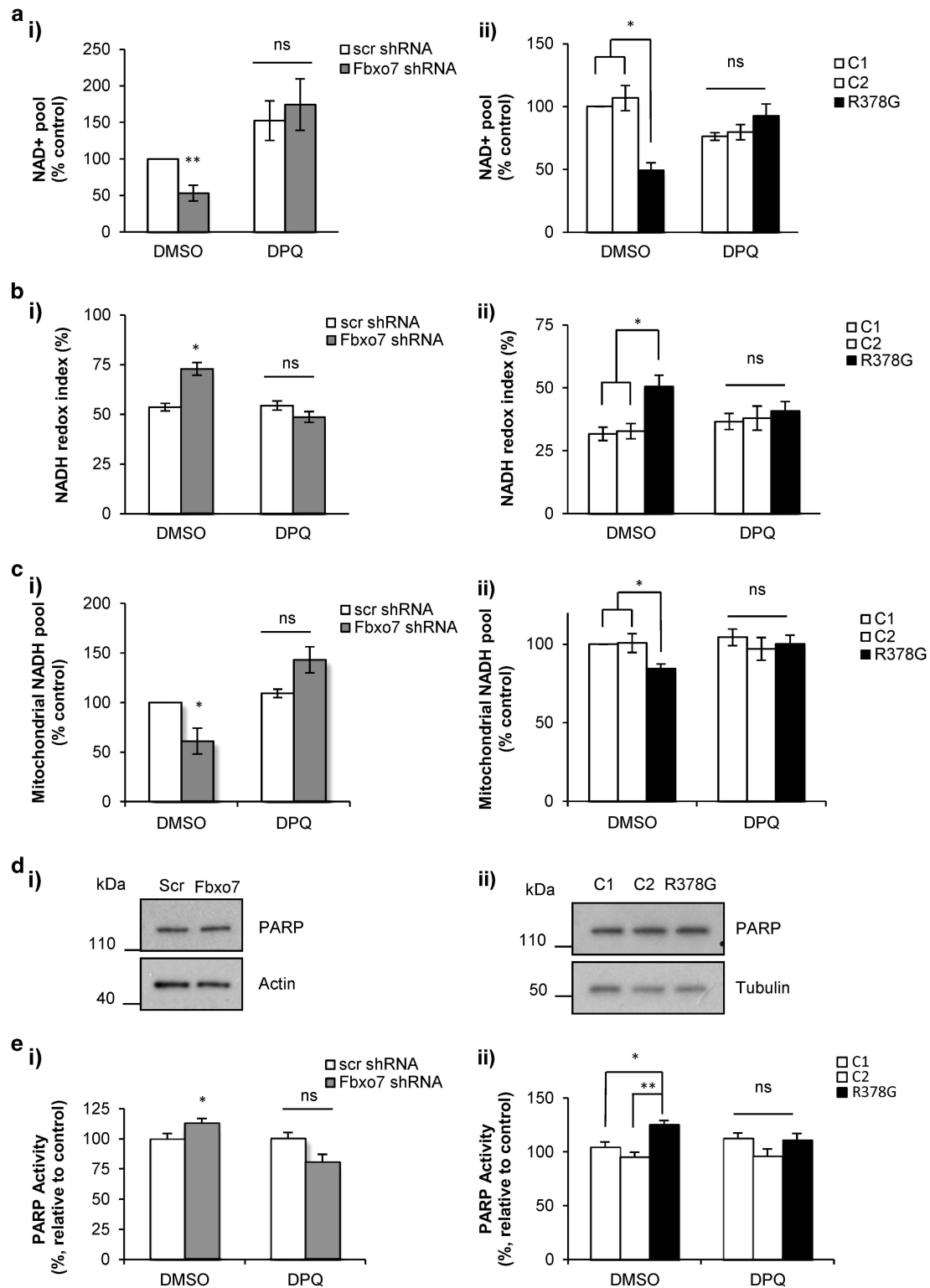
Figure 5 For caption please refer page 128

homeostasis and floods with calcium.[40,41] A sharp rise in Mag-Fura ratio therefore indicates a bioenergetic collapse. Application of 1 mM NaCN (inhibitor of mitochondrial respiration) and inhibitor of glycolysis iodoacetic acid (IAA; 100 μM) completely blocked ATP production in these cells.

Consumption of ATP in cells led to depletion of ATP pool and then cell collapse, which can be recorded as a massive increase in Mag-Fura ratio (Figure 6bi). In agreement with [ATP] data presented in Figure 1c, we found that *Fbxo7* KD cells have a shorter time to collapse (54.01 ± 1.92 min,

Figure 5 Fbxo7 deficiency increased PARP activity; PARP inhibitor DPQ restored NAD$^+$ pool, NADH redox index and mitochondrial NADH pool in these cells. (**a**) Cellular NAD$^+$ levels were measured using a colorimetric cell-based assay kit. Histograms represent average cellular NAD$^+$ content $\pm$ S.E.M per protein concentration normalised to control cells in (**ai**) SH-SY5Y cells stably expressing either scr or Fbxo7 shRNA, and (**aii**) control and patient fibroblasts treated with either DMSO or DPQ for 24 h. (**b**) Histograms represent the mean of the mitochondrial redox index in SH-SY5Y cells expressing either (**bii**) scr or Fbxo7 shRNA, and (**bii**) control and patient fibroblasts with *Fbxo7* R378G mutation. (**c**) Mitochondrial NADH pool was calculated and normalised to control cells for (**ci**) *Fbxo7* KD SH-SY5Y cells and (**cii**) patient fibroblasts. In all cases ** indicates $P < 0.01$; *$P < 0.05$; NS, not significant; $n > 4$ independent experiments. (**d**) PARP enzyme levels were assessed by western blot in cell lysates from SH-SY5Y, expressing either Scr or Fbxo7 shRNA (**di**) and in fibroblasts from control individuals and a patient with *Fbxo7* R378G mutation (**dii**). Only one band was detected, corresponding to full length PARP. (**e**) PARP1 activity was measured using the HT Colorimetric PARP/Apoptosis Assay from Trevigen (Gaithersburg, MD, USA), as described in Methods, in SHSY5Y cells (**ei**) and fibroblasts (**eii**) treated with vehicle (DMSO) or PARP1 inhibitor DPQ 10 μM for 24 h. Results were normalised to PARP activity of control in every experiment. In all cases data are represented as mean $\pm$ S.E.M.; ** indicates $P < 0.01$; *$P < 0.05$; n.s, not significant; $n \geq 4$ independent experiments
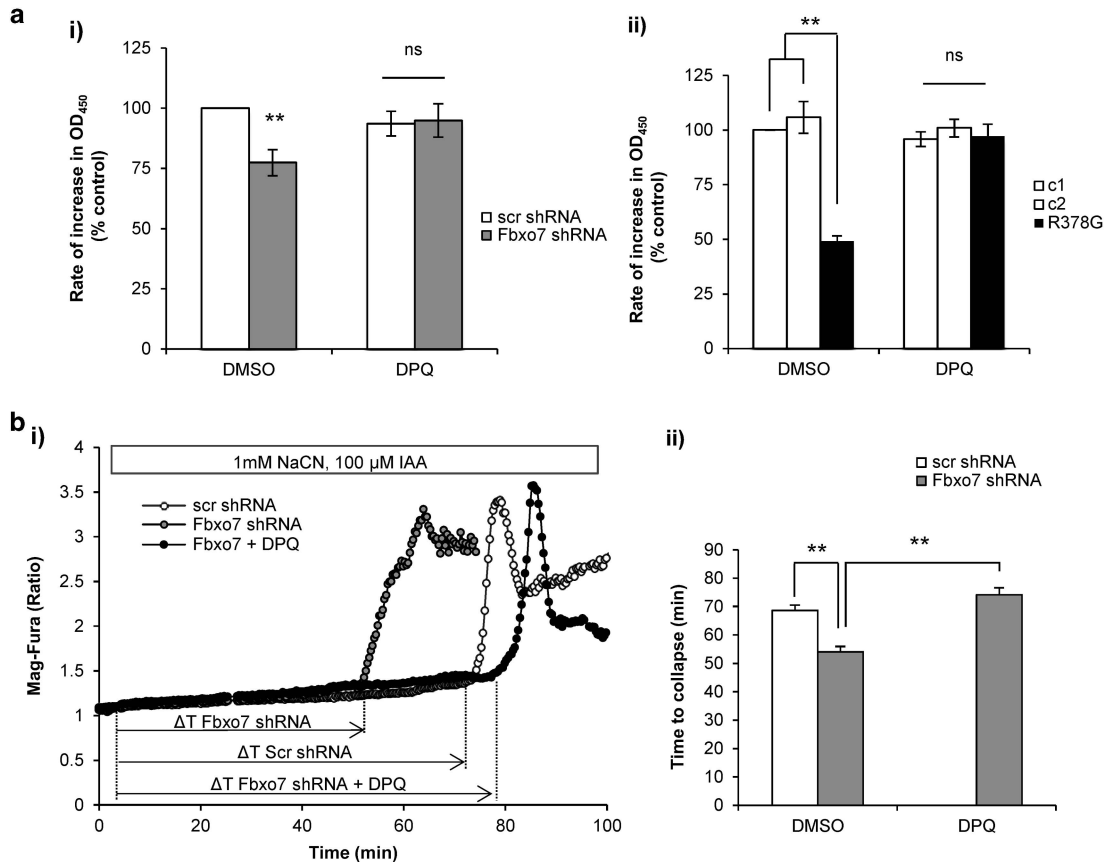

Figure 6 DPQ PARP inhibitor restores NADH dehydrogenase activity of isolated complex I and increases ATP pool in Fbxo7-deficient cells. (**a**) Complex I NADH dehydrogenase activity was measured kinetically over 30 min and the rate was determined as change in optical density over time. Rate of complex I activity was calculated and normalised to control cells for (**ai**) *Fbxo7* KD SH-SY5Y cells and (**aii**) patient fibroblasts; **$P < 0.01$. The experiment was performed $n > 3$. Data are represented as mean $\pm$ S.E.M. (**b**) ATP levels were assessed using the Mg^{2+} indicator Mag-Fura. Inhibition of ATP production by blocking mitochondrial respiration with 1 mM NaCN and glycolysis with 100 μM iodoacetic acid (IAA) induced a consumption of ATP resulting in slow increase in Mag-Fura ratio and bioenergetic cell collapse, when ATP is completely depleted (which resulted in high increase in Mag-Fura ratio due to calcium overload). Representative traces of the experiment are shown in (**bi**). Time to collapse was calculated for each condition and represented in (**bii**) (data represent mean $\pm$ S.E.M, **$P < 0.01$)

$n = 41$ cells) compared with control (68.60 ± 1.87 min, $n = 89$ cells; $P < 0.01$; Figure 6bii). Treatment with the PARP inhibitor DPQ (10 μM) significantly delayed the time to cell collapse after inhibition of ATP production (to 74.16 ± 2.44 min, $n = 42$ cells; Figure 6bi–ii), suggesting restoration of ATP pool in these cells.

Discussion

Complex I deficiency has been reported in various tissues from patients with idiopathic PD.[42] PARP upregulation has been previously implicated in PD pathogenesis and its

inhibition has been shown to protect against cytotoxicity in the MPTP model of PD.[43–45] PARP-mediated cell death has also been associated with mitochondrial dysfunction,[46,47] though the downstream events of PARP activation remain to be fully characterised. Previous studies have reported that prolonged PARP activation results in inhibition of the glycolytic pathway caused by a reduction in NAD$^+$ content, which subsequently compromises respiration where NADH is a key cofactor.[33,48] We also show that in *Fbxo7* KD SH-SY5Ys and R378G mutant fibroblasts, NAD$^+$ levels are reduced and can be restored after DPQ treatment, strongly suggesting that a limitation in

NAD^{+} bioavailability is associated with PARP-linked respiratory impairment. Another study, however, has reported that the bioenergetic collapse following PARP activation is not dependent on NAD^{+} depletion, but instead on reduced glycolysis through PAR-dependent hexokinase inhibition.[49] This has then been confirmed by another study showing that PARP-mediated PAR synthesis results in reduced glycolysis and ATP loss.[50] PARP activity has also been suggested to reduce respiration by direct influence on the enzymatic activity of mitochondrial proteins.[51,52] Though PARP localisation is predominantly nuclear, PARP and PARylation events have been detected at the mitochondria.[51,52] Regardless of the glycolytic maintenance, heterologous expression of a truncated active form of PARP containing a MTS has been shown to cause accumulation of mitochondrial PARylation and inhibit respiration, suggesting that PARP activity on its own is sufficient to cause mitochondrial dysfunction.[52]

PARP-associated mitochondrial dysfunction can also result from inhibition of other enzymes implicated in the regulation of energy balance. Sirtuin1 (SIRT1) stimulates mitochondrial biogenesis by regulation of PGC-1α,[53] and has been linked with mitophagy by direct deacetylation of autophagy mediators and deacetylation of the FOXO family of transcription factors.[54,55] SIRT3 deacetylates ETC proteins, including complex I,[56,57] and modulates hexokinase II dissociation from the mitochondria increasing oxidative phosphorylation.[58] Excessive PARP activation has been reported to repress SIRT activity by depletion of cellular NAD^{+} or by transcriptional downregulation.[59] Complex I-driven respiration in Fbxo7-deficient cells may thus not only result from direct PARylation and PARP-mediated cellular NAD^{+} decrease, but also from its effect on substrate PARylation and SIRT activity.

Fbxo7 deficiency is associated with mitochondrial dysfunction, either through impairment of mitochondrial respiration or accumulation of defective mitochondria via impaired mitophagy, it is plausible that PARP upregulation is a common downstream effect of one or more of these impaired mitochondrial mechanisms in Fbxo7 deficiency, where ROS dependent (mitochondrial) DNA damage may be active. These findings suggest PARP inhibitors as a potential drug treatment in PD and other mitochondria-associated neurodegenerative disorders.

Materials and Methods

Cell culture. SH-SY5Y cells were purchased from the European Collection of Cell Cultures (Health Protection Agency, Salisbury, UK) and cultured at 37 °C and 5% CO_2 in Dulbecco's modified Eagle medium (DMEM) containing high glucose, sodium pyruvate and 2 mM L-glutamine, (Invitrogen, Carlsbad, CA, USA), supplemented with 10% (v/v) foetal bovine serum (FBS; PAA). With informed consent, fibroblasts were obtained from an upper arm punch biopsy taken from healthy and an affected individual carrying the homozygous *Fbxo7* R378G mutation. The tissue was dissected and cultured in 5 cm[2] Petri dishes until fibroblasts grew confluent enough to be transferred and cultured in larger culture vessels containing DMEM with GlutaMAX, high glucose, sodium pyruvate and supplemented with 10% (v/v) FBS (PAA) and 1% streptomycin (Sigma-Aldrich, St. Louis, MO, USA). Where indicated, cells were treated with 10 μM DPQ for the appropriate time period before harvesting lysates or live imaging.

Construct generation. Transient scr and *Fbxo7* KD SH-SY5Y cells were generated by transfecting either non-targeting scramble siRNA or a pool of four siRNA constructs targeting human *Fbxo7* (siGenome SMARTpool) using

Dharmafect transfection reagent (Dharmacon, Lafayette, CO, USA; Thermo Fisher Scientific, Waltham, MA, USA). Scr and *Fbxo7* KD shRNA SH-SY5Y cells were produced by retroviral infection with two independent miR30-based short hairpin constructs against either bp 387–404 or bp 444–460 of Fbxo7 isoform 1 (constructs generated in-house38). Silencing was maintained in stable cell lines by the addition of 1 μg/ml puromycin to the growth medium.

Measurement of $\Delta\Psi$m. $\Delta\Psi$m was measured by fluorescence imaging in cells preincubated for 40 min at room temperature (RT) with 25 nM TMRM (Invitrogen) resuspended in Hank's balanced salt solution (HBSS; 156 mM NaCl, 3 mM KCl, 2 mM MgSO$_4$, 1.25 mM KH$_2$PO$_4$, 2 mM CaCl$_2$, 10 mM glucose and 10 mM HEPES; pH adjusted to 7.35 with NaOH) and kept in the media throughout the recording time. Z-stack confocal images were acquired using a Zeiss 710 VIS CLSM confocal microscope equipped with a META detection system and an ×40 oil immersion objective (Zeiss, Oberkochen, Germany) and analysed using Zeiss software (Zeiss). The 560 nm laser line was used to excite TMRM and fluorescence was measured above 580 nm. For analysis of the effect of mitochondrial toxins on $\Delta\Psi$m, images were recorded continuously from a single focal plane. All imaging data was exported and analysed using Volocity 3D image analysis software (PerkinElmer, Waltham, MA, USA). To reduce background, the average intensity measurements of each image was selected above a threshold intensity adjusted manually for each experiment and applied to each image collected in an experiment. For each individual experiment, average TMRM fluorescence was normalised to control cells to allow comparison between different-day experiments. TMRM is used in the redistribution mode to assess $\Delta\Psi_m$, thus a reduction in TMRM fluorescence represents mitochondrial depolarisation. To avoid any effects of the multi drug resistance pore on TMRM loading, in some experiments cells were treated with 5 μM cyclosporine H.

Measurement of cellular ATP content. Total cellular levels of ATP were measured using the Vialight plus assay kit (Lonza, Verviers, Belgium) based on the luminescence reaction that results from the oxidation of luciferin to oxyluciferin by the firefly luciferase in an ATP-dependent manner. Approximately 500 000 cells per well were plated in a luminescence compatible 96-well format. Cells were washed in HBSS and lysed for 10 min in 50 μl of lysis buffer provided by the supplier. A measure of 100 μl of ATP monitoring reagent Plus were then added to each well and incubated at RT to generate the luminescence signal. After 2 min the luminescent reaction was measured using a FLUOstar omega plate reader (BMG Labtech Ltd, Ortenberg, Germany) with a specialised luminescence head. To determine the ATP concentration, all samples were referred to an ATP standard curve with known concentrations ranging from 1×10^{-11} M to 1×10^{-6} M and normalised to protein concentration.

Measurement of oxygen consumption. Oxygen consumption rate was measured using a Clark-type oxygen electrode thermostatically maintained at 37°C. Approximately 5×10^7 cells were resuspended in respiration buffer (HBSS containing D-glucose; 10 mM) and kept on ice before the time of recording. The electrode was first calibrated by addition of air-saturated water assuming to contain 406 nmol O atoms/ml at 37 °C. A measure of 50 μl of cells in suspension were added to the chamber containing 200 μl of respiration buffer and the rate of oxygen consumption was monitored in the graph generated by Oxygraph Plus system software (Hansatech Instruments, King's Lynn, Norfolk, UK). Once the signal value stabilised for 1–3 min, the basal rate of oxygen consumption driven by internal substrate oxidation was recorded from the cells. Oligomycin (2 μg/ml) was then added to inhibit ATP synthase and reduce the rate of consumption; FCCP (1 μM) was then added to maximise respiration and determine the maximal rate of oxygen consumption.

For measurement of the activity of individual respiratory complexes, cells were permeabilised with digitonin (40 μM) and resuspended in mitochondrial respiration buffer (135 mM KCl, 10 mM NaCl, 20 mM HEPES, 0.5 mM KH$_2$PO$_4$, 1 mM MgCl$_2$, 5 mM EGTA and 1.86 mM CaCl$_2$; pH 7.1). At the time of recording, the Clark-type oxygen electrode was thermostatically maintained at 25 °C. A measure of 50 μl of cell suspension were added to the chamber containing already 200 μl of mitochondrial respiration buffer with substrates for complex I (glutamate and malate 5 mM) or complex II (succinate 5 mM with rotenone 5 μM). After recording for 1–2 min, 50 nmoles ADP were added to stimulate ATP synthesis, thereby increasing the rate of oxygen consumption (state III respiration). Upon consumption of ADP, respiration was reduced and rate of oxygen consumption reached a state of plateau (state IV). All data were obtained using an Oxygraph Plus system with chart recording software.

Measurement of cytosolic ROS. Cells plated on 25 mM glass coverslips were loaded with the fluorescent probe DHE (80 μM; Molecular Probes, Invitrogen) in HBSS and kept present in the solution during the experiment. No preincubation was done for DHE to minimise accumulation of oxidised products. ROS production was monitored in single cells using light from a Xenon arc lamp passed through a monochromator to provide excitation light sequentially at 380 and 530 nm. Emitted light was reflected through a 455 or 605 nm long-pass filter to a cooled CCD camera. Rate of ROS production is proportional to the rate of increase in the ratio of 530/380 nm fluorescence. Images were captured and analysed using IQM software from Andor (Belfast, UK).

Measurement of isolated complex I NADH dehydrogenase activity. The NADH dehydrogenase activity of isolated complex I was measured using the complex I enzyme activity microplate assay kit (Abcam, Cambridge, UK). Cells cultured in 10 cm^2 dish were lysed in lysis buffer provided by the manufacturer and transferred into an eppendorf left on ice for ~ 20 min to allow protein extraction. Samples were then centrifuged at 12 000xg for 20 min at 4 °C and total protein concentration in the supernatant was estimated using Pierce BCA Protein Assay Kit (Thermo Fisher Scientific). Samples were then diluted in incubation solution (provided by the manufacturer) to reach a final protein concentration of 0.5 μg/μl. A measure of 200 μl of each sample were transferred to each well of the microplate containing immobilised anti-complex I antibody bound to the wells and incubated for 3 h at RT. After the incubation period, the wells were rinsed twice in 300 μl of buffer, provided by the manufacturer, and 200 μl of assay solution containing NADH and a reporter dye were added to each well. NADH dehydrogenase activity was determined by measuring the oxidation of exogenous NADH to NAD$^+$, coupled to the 1 : 1 reduction of the reporter dye of which product concentration was proportional to the increase in absorbance at 450 nm, measured over time using a spectrophotometer. Complex I activity was expressed as the rate of increase in absorbance per amount of sample loaded in the well.

Immunoblotting. Immunoblotting was performed as described previously.[10] Anti-human β-actin mouse monoclonal antibody (dilution 1:10 000) was obtained from Sigma-Aldrich; anti-Fbxo7 rabbit polyclonal antibody (dilution 1 : 1000) was obtained from Novus Biologicals (Littleton, CO, USA); total OXPHOS cocktail mouse monoclonal antibody (dilution 1 : 1000) was obtained from Mitosciences. Anti-human PARP polyclonal antibody (1 : 1000) was obtained from Cell Signaling (Danvers, MA, USA). Rabbit and mouse secondary antibodies were purchased from Santa Cruz Biotechnology ((Santa Cruz, CA, USA) dilution 1 : 2000). All primary and secondary antibodies were diluted in 5% (w/v) milk PBS–Tween.

Measurement of NADH and FAD^{++} redox indexes. NADH autofluorescence was measured in cells plated on 25 mM glass coverslips using an epifluorescence-inverted microscope equipped with a × 20 fluorite objective. For measurement of NADH in single cells, excitation light at a wavelength of 350 nm was provided by a Xenon arc lamp, the beam passing through a monochromator (Cairn Research, Faversham, Kent, UK). Emitted fluorescence light was reflected through a 455 nm long-pass filter to a cooled CCD camera (Retiga, QImaging, Surrey, BC, Canada) and digitised to 12 bit resolution. All imaging data was collected and analysed using software from Andor. FAD^{++} autofluorescence was measured in cells plated on 25 mM glass coverslips using a Zeiss 710 VIS CLSM confocal microscope equipped with a META detection system and a × 40 oil immersion objective. The excitation light was provided at a wavelength of 454 nm and fluorescence was measured from 505–550 nm. Illumination intensity was kept to a minimum (at 0.1–0.2% of laser output) to avoid phototoxicity and the pinhole set to give an optical slice of ~ 2 μm. Basal autofluorescence was normalised between the minimal signal (set to 0%) and maximal signal (set to 100%), generated in response to the respiratory inhibitor NaCN (1 mM) and the uncoupler FCCP (1 μM), respectively.

Measurement of free cytosolic magnesium. For measurements of $[Mg^{2+}]_c$, cells were loaded for 30 min at RT with 5 μM Mag-Fura-AM (Molecular Probes, Invitrogen) and 0.005% pluronic acid in HBSS. Mag-Fura fluorescence was monitored in single cells using excitation light provided by a Xenon arc lamp, the beam passing through a monochromator at 340 and 380 nm (Cairn Research, Kent, UK). Emitted fluorescence light was reflected through a 515 nm long-pass filter to a cooled CCD camera (Retiga, QImaging, Canada) and digitised to 12 bit resolution. All imaging data were collected and analysed using software from Andor (Belfast, UK). Traces, obtained using the cooled CCD imaging system, are presented as the ratio of excitation at 340 and 380 nm, both with emission at > 515 nm.

PARP activity. PARP activity was determined using the HT Colorimetric PARP/Apoptosis Assay from Trevigen. The kit is an ELISA that detects PAR deposited onto immobilised histone proteins. Cells were grown on a 24-well plate and treated with DPQ 10 μM or vehicle (DMSO) for 24 h. Cells were washed with PBS and lysates were prepared using the cell extraction buffer provided. Protein concentration was estimated using BCA Protein Assay kit and lysates were diluted with cell lysis buffer to a concentration of 25 ng/μl for fibroblasts and 8 ng/μl for SHSY5Y cells. A measure of 25 μl were then transferred in duplicate to a well of the ELISA plate and the assay was performed following manufacturer instructions. PARP activity correlates with the absorbance of the colorimetric signal generated, which was quantified at 450 nm using a FLUOstar Omega Microplate Reader (BMG Labtech Ltd).

Measurement of cellular NAD$^+$ levels. Intracellular NAD$^+$ levels were measured using a colorimetric cell-based assay kit (Cayman Chemical). Cells were cultured in a 96-well plate and resuspended in lysis buffer, provided by the manufacturer. After 30 min of gentle shaking at RT, the plate was centrifuged at 1000 × g for 10 min at 4 °C and 100 μl of each cell lysate were transferred into corresponding wells of a new plate. A measure of 100 μl of reaction solution were added to each well and incubated with gentle shaking at RT. After 1.5 h, the absorbance in each well was measured using a microplate reader at wavelength of 450 nm. The NAD$^+$ concentration in each sample was referred to a standard curve with known concentrations of NAD$^+$ and normalised to protein concentration.

Statistical analysis. Statistical analysis was performed using GraphPad Prism 6 software (La Joya, CA, USA). Data were analysed by Student's t-test or ANOVA followed by Tukey's test correction, and statistical significance is expressed as * $P < 0.05$, **$P < 0.01$, ***$P < 0.005$. Data were generated from a minimum of three independent experiments, and for all graphs, error bars represent mean $\pm$ S.E.M.

Conflict of Interest

The authors declare no conflict of interest.

1. Burchell VS, Gandhi S, Deas E, Wood NW, Abramov AY, Plun-Favreau H. Targeting mitochondrial dysfunction in neurodegenerative disease: part II. *Expert Opin Ther Targets* 2010; **14**: 497–511.
2. Bekris LM, Mata IF, Zabetian CP. The genetics of Parkinson disease. *J Geriatr Psychiatry Neurol* 2010; **23**: 228–242.
3. Martinez TN, Greenamyre JT. Toxin models of mitochondrial dysfunction in Parkinson's disease. *Antioxid Redox Signal* 2012; **16**: 920–934.
4. Hisahara S, Shimohama S. Toxin-induced and genetic animal models of Parkinson's disease. *Parkinsons Dis* 2010; **2011**: 951709.
5. Hargreaves IP, Lane A, Sleiman PMA. The coenzyme Q10 status of the brain regions of Parkinson's disease patients. *Neurosci Lett* 2008; **447**: 17–19.
6. Parker WD, Parks JK, Swerdlow RH. Complex I deficiency in Parkinson's disease frontal cortex. *Brain Res* 2008; **1189**: 215–218.
7. Schapira AH V. Mitochondria in the aetiology and pathogenesis of Parkinson's disease. *Lancet Neurol* 2008; **7**: 97–109.
8. Abramov AY, Gegg M, Grunewald A, Wood NW, Klein C, Schapira AHV. Bioenergetic consequences of PINK1 mutations in Parkinson disease. *PLoS One* 2011; **6**: e25622.
9. Björkblom B, Maple-Grødem J, Puno MR, Odell M, Larsen JP, Møller SG. Reactive oxygen species-mediated DJ-1 monomerization modulates intracellular trafficking involving karyopherin β2. *Mol Cell Biol* 2014; **34**: 3024–3040.
10. Fitzgerald JC, Camprubi MD, Dunn L, Wu H-C, Ip NY, Kruger R *et al.* Phosphorylation of HtrA2 by cyclin-dependent kinase-5 is important for mitochondrial function. *Cell Death Differ* 2012; **19**: 257–266.
11. Pickrell AM, Youle RJ. The roles of PINK1, parkin, and mitochondrial fidelity in Parkinson's disease. *Neuron* 2015; **85**: 257–273.
12. Di Fonzo A, Dekker MCJ, Montagna P, Baruzzi A, Yonova EH, Correia Guedes L *et al.* FBXO7 mutations cause autosomal recessive, early-onset parkinsonian-pyramidal syndrome. *Neurology* 2009; **72**: 240–245.
13. Skowyra D, Craig KL, Tyers M, Elledge SJ, Harper JW. F-box proteins are receptors that recruit phosphorylated substrates to the SCF ubiquitin-ligase complex. *Cell* 1997; **91**: 209–219.

14. Bai C, Sen P, Hofmann K, Ma L, Goebl M, Harper JW *et al.* SKP1 connects cell cycle regulators to the ubiquitin proteolysis machinery through a novel motif, the F-box. *Cell* 1996; **86**: 263–274.

15. Nelson DE, Randle SJ, Laman H. Beyond ubiquitination: the atypical functions of Fbxo7 and other F-box proteins. *Open Biol* 2013; **3**: 130131.

16. Burchell VS, Nelson DE, Sanchez-Martinez A, Delgado-Camprubi M, Ivatt RM, Pogson JH *et al.* The Parkinson's disease-linked proteins Fbxo7 and Parkin interact to mediate mitophagy. *Nat Neurosci* 2013; **16**: 1257–1265.

17. Moroni F. Poly(ADP-ribose)polymerase 1 (PARP-1) and postischemic brain damage. *Curr Opin Pharmacol* 2008; **8**: 96–103.

18. Diefenbach J, Bürkle A. Introduction to poly(ADP-ribose) metabolism. *Cell Mol Life Sci* 2005; **62**: 721–730.

19. Abeti R, Abramov AY, Duchen MR. Beta-amyloid activates PARP causing astrocytic metabolic failure and neuronal death. *Brain* 2011; **134**(Pt 6): 1658–1672.

20. Cecchi C, Fiorillo C, Sorbi S, Latorraca S, Nacmias B, Bagnoli S *et al.* Oxidative stress and reduced antioxidant defenses in peripheral cells from familial Alzheimer's patients. *Free Radic Biol Med* 2002; **33**: 1372–1379.

21. Love S, Barber R, Wilcock GK. Increased poly(ADP-ribosyl)ation of nuclear proteins in Alzheimer's disease. *Brain* 1999; **122**(Pt 2): 247–253.

22. Abramov AY, Duchen MR. Mechanisms underlying the loss of mitochondrial membrane potential in glutamate excitotoxicity. *Biochim Biophys Acta* 2008; **1777**: 953–964.

23. Duan Y, Gross RA, Sheu S-S. Ca2+-dependent generation of mitochondrial reactive oxygen species serves as a signal for poly(ADP-ribose) polymerase-1 activation during glutamate excitotoxicity. *J Physiol* 2007; **585**(Pt 3): 741–758.

24. Brand MD, Nicholls DG. Assessing mitochondrial dysfunction in cells. *Biochem J* 2011; **435**: 297–312.

25. Adachi K, Oiwa K, Nishizaka T, Furuike S, Noji H, Itoh H *et al.* Coupling of rotation and catalysis in F(1)-ATPase revealed by single-molecule imaging and manipulation. *Cell* 2007; **130**: 309–321.

26. Jonckheere AI, Smeitink JAM, Rodenburg RJT. Mitochondrial ATP synthase: architecture, function and pathology. *J Inherit Metab Dis* 2012; **35**: 211–225.

27. Berndt N, Holzhütter H-G, Bulik S. Implications of enzyme deficiencies on mitochondrial energy metabolism and reactive oxygen species formation of neurons involved in rotenone-induced Parkinson's disease: a model-based analysis. *FEBS J* 2013; **280**: 5080–5093.

28. Murphy MP. How mitochondria produce reactive oxygen species. *Biochem J* 2009; **417**: 1–13.

29. Tretter L, Sipos I, Adam-Vizi V. Initiation of neuronal damage by complex I deficiency and oxidative stress in Parkinson's disease. *Neurochem Res* 2004; **29**: 569–577.

30. Bartolomé F, Abramov AY. Measurement of mitochondrial NADH and FAD autofluorescence in live cells. *Methods Mol Biol* 2015; **1264**: 263–270.

31. Gandhi S, Wood-Kaczmar A, Yao Z, Plun-Favreau H, Deas E, Klupsch K *et al.* PINK1-associated Parkinson's disease is caused by neuronal vulnerability to calcium-induced cell death. *Mol Cell* 2009; **33**: 627–638.

32. Houtkooper RH, Cantó C, Wanders RJ, Auwerx J. The secret life of NAD+: an old metabolite controlling new metabolic signaling pathways. *Endocr Rev* 2010; **31**: 194–223.

33. Alano CC, Garnier P, Ying W, Higashi Y, Kauppinen TM, Swanson RA. NAD+ depletion is necessary and sufficient for poly(ADP-ribose) polymerase-1-mediated neuronal death. *J Neurosci* 2010; **30**: 2967–2978.

34. Bai P, Cantó C. The role of PARP-1 and PARP-2 enzymes in metabolic regulation and disease. *Cell Metab* 2012; **16**: 290–295.

35. Wang S, Yang X, Lin Y, Qiu X, Li H, Zhao X *et al.* Cellular NAD depletion and decline of SIRT1 activity play critical roles in PARP-1-mediated acute epileptic neuronal death *in vitro*. *Brain Res* 2013; **1535**: 14–23.

36. Wang S, Xing Z, Vosler PS, Yin H, Li W, Zhang F *et al.* Cellular NAD replenishment confers marked neuroprotection against ischemic cell death: role of enhanced DNA repair. *Stroke* 2008; **39**: 2587–2595.

37. Scalia M, Satriano C, Greca R, Stella AMG, Rizzarelli E, Spina-Purrello V. PARP-1 inhibitors DPQ and PJ-34 negatively modulate proinflammatory commitment of human glioblastoma cells. *Neurochem Res* 2013; **38**: 50–58.

38. Song Z-F, Ji X-P, Li X-X, Wang S-J, Wang S-H, Zhang Y. Inhibition of the activity of poly (ADP-ribose) polymerase reduces heart ischaemia/reperfusion injury via suppressing JNK-mediated AIF translocation. *J Cell Mol Med* 2008; **12**: 1220–1228.

39. Wang G, Huang X, Li Y, Guo K, Ning P, Zhang Y. PARP-1 inhibitor, DPQ, attenuates LPS-induced acute lung injury through inhibiting NF-κB-mediated inflammatory response. *PLoS One* 2013; **8**: e79757.

40. Abramov AY, Duchen MR. Impaired mitochondrial bioenergetics determines glutamate-induced delayed calcium deregulation in neurons. *Biochim Biophys Acta* 2010; **1800**: 297–304.

41. Plun-Favreau H, Burchell VS, Holmström KM, Yao Z, Deas E, Cain K *et al.* HtrA2 deficiency causes mitochondrial uncoupling through the F_1F_1-ATP synthase and consequent ATP depletion. *Cell Death Dis* 2012; **3**: e335.

42. Schapira AH, Cooper JM, Dexter D, Jenner P, Clark JB, Marsden CD. Mitochondrial complex I deficiency in Parkinson's disease. *Lancet* 1989; **1**: 1269.

43. Lee Y, Karuppagounder SS, Shin J-H, Lee Y-I, Ko HS, Swing D *et al.* Parthanatos mediates AIMP2-activated age-dependent dopaminergic neuronal loss. *Nat Neurosci* 2013; **16**: 1392–1400.

44. Martire S, Mosca L, d'Erme M. PARP-1 involvement in neurodegeneration: A focus on Alzheimer's and Parkinson's diseases. *Mech Ageing Dev* 2015; **146–148C**: 53–64.

45. Outeiro TF, Grammatopoulos TN, Altmann S, Amore A, Standaert DG, Hyman BT *et al.* Pharmacological inhibition of PARP-1 reduces alpha-synuclein- and MPP+-induced cytotoxicity in Parkinson's disease in vitro models. *Biochem Biophys Res Commun* 2007; **357**: 596–602.

46. Chen M, Zsengellér Z, Xiao C-Y, Szabó C. Mitochondrial-to-nuclear translocation of apoptosis-inducing factor in cardiac myocytes during oxidant stress: potential role of poly (ADP-ribose) polymerase-1. *Cardiovasc Res* 2004; **63**: 682–688.

47. Yu S-W, Wang H, Poitras MF, Coombs C, Bowers WJ, Federoff HJ *et al.* Mediation of poly (ADP-ribose) polymerase-1-dependent cell death by apoptosis-inducing factor. *Science* 2002; **297**: 259–263.

48. Ying W, Garnier P, Swanson RA. NAD+ repletion prevents PARP-1-induced glycolytic blockade and cell death in cultured mouse astrocytes. *Biochem Biophys Res Commun* 2003; **308**: 809–813.

49. Andrabi SA, Umanah GKE, Chang C, Stevens DA, Karuppagounder SS, Gagné J-P *et al.* Poly(ADP-ribose) polymerase-dependent energy depletion occurs through inhibition of glycolysis. *Proc Natl Acad Sci USA* 2014; **111**: 10209–10214.

50. Fouquerel E, Goellner EM, Yu Z, Gagné J-P, Barbi de Moura M, Feinstein T *et al.* ARTD1/PARP1 negatively regulates glycolysis by inhibiting hexokinase 1 independent of NAD(+) depletion. *Cell Rep* 2014; **8**: 1819–1831.

51. Baek S-H, Bae O-N, Kim E-K, Yu S-W. Induction of mitochondrial dysfunction by poly(ADP-ribose) polymer: implication for neuronal cell death. *Mol Cell* 2013; **36**: 258–266.

52. Niere M, Kernstock S, Koch-Nolte F, Ziegler M. Functional localization of two poly(ADP-ribose)-degrading enzymes to the mitochondrial matrix. *Mol Cell Biol* 2008; **28**: 814–824.

53. Lagouge M, Argmann C, Gerhart-Hines Z, Meziane H, Lerin C, Daussin F *et al.* Resveratrol improves mitochondrial function and protects against metabolic disease by activating SIRT1 and PGC-1alpha. *Cell* 2006; **127**: 1109–1122.

54. Lee IH, Cao L, Mostoslavsky R, Lombard DB, Liu J, Bruns NE *et al.* A role for the NAD-dependent deacetylase Sirt1 in the regulation of autophagy. *Proc Natl Acad Sci USA* 2008; **105**: 3374–3379.

55. Brunet A, Sweeney LB, Sturgill JF, Chua KF, Greer PL, Lin Y *et al.* Stress-dependent regulation of FOXO transcription factors by the SIRT1 deacetylase. *Science* 2004; **303**: 2011–2015.

56. Ahn B-H, Kim H-S, Song S, Lee IH, Liu J, Vassilopoulos A *et al.* A role for the mitochondrial deacetylase Sirt3 in regulating energy homeostasis. *Proc Natl Acad Sci USA* 2008; **105**: 14447–14452.

57. Finley LWS, Haas W, Desquiret-Dumas V, Wallace DC, Procaccio V, Gygi SP *et al.* Succinate dehydrogenase is a direct target of sirtuin 3 deacetylase activity. *PLoS One* 2011; **6**: e23295.

58. Shulga N, Pastorino JG. Hexokinase II binding to Mitochondria is Necessary for Kupffer cell Activation and is Potentiated by Ethanol Exposure. *J Biol Chem* 2014; **289**: 26213–2.

59. Cantó C, Auwerx J. Targeting sirtuin 1 to improve metabolism: all you need is NAD(+)? *Pharmacol Rev* 2012; **64**: 166–187.

Supplementary Information accompanies this paper on *Cell Death and Differentiation* website (http://www.nature.com/cdd)